Enhanced catalytic activity for NO oxidation over Ba doped $LaCoO_3$ catalyst

Chen Zhou,[a] Zijian Feng,[b] Yexin Zhang,[a] Lingjun Hu,[a] Rong Chen,[c] Bin Shan,*[b] Hongfeng Yin,*[a] Wei Guo Wang[a] and Aisheng Huang[a]

A series of $La_{1-x}Ba_xCoO_3$ ($x = 0$, 0.1, 0.2, 0.3) perovskites were synthesized by the modified sol–gel method, and their activities for NO oxidation were investigated as well. The relevant structural characterizations of the prepared catalysts were conducted by XRD, ICP, BET, FTIR, TEM, H_2-TPR and NO-TPD. The performance evaluation indicated that introduction of Ba at the A-site in $LaCoO_3$ greatly improved the activity for NO oxidation. The best performance with NO conversion of 93% at 265 °C was obtained on $La_{0.9}Ba_{0.1}CoO_3$. Additionally, the Ba-doped $LaCoO_3$ had better performance than that of the classical Pt/Al_2O_3 catalyst, implying that the non-noble catalysts could be considered as potential substituting candidates for noble metal-based catalysts.

1. Introduction

Considering a better fuel economy and power output, lean-burn engines have attracted more attention than conventional engines.[1,2] However, it is difficult to eliminate NOx under the lean-burn conditions on account of the lack of reductants. Therefore the abatement of NOx becomes quite critical due to the increasing NOx emission regulations because of their harm to human-beings and the environment. At present, selective catalytic reduction (SCR) and lean NOx trap (LNT) are two main technologies for NOx removal.[3–6] For SCR technology, the presence of NO_2 can promote NOx removal.[7,8] As to LNT technology, also named NOx Storage–Reduction (NSR), NO_2 are more effective to be absorbed on catalysts as nitrates than NO. Consequently, the conversion of NO to NO_2 is of importance for NOx removal.[6,9] At this instance, the conventional noble metal-based catalysts are employed. A substitution to conventional catalyst needs to be developed due to lower stability and high cost of noble metals.

In the last decades, much attention has been paid to the catalysts derived from perovskite structures with general formula ABO_3, where A is a rare earth cation and B is a transition metal (Co, Ni, Fe or Mn).[10–18] During the NOx removal process, the ability for the oxidation of NO to NO_2 is significant. $LaMO_3$ (M = Co, Mn, Fe) perovskites were ever studied as NO oxidation catalysts and Co-based catalysts exhibited better catalytic activity.[2] Kim *et al.* investigated a mixture of $La_{0.9}Sr_{0.1}MO_3$ (M = Mn, Co) and Pd–Rh/BaO/CeO_2–ZrO_2 to rival a commercial Pt-containing LNT catalyst, it was noteworthy that $La_{0.9}Sr_{0.1}MO_3$ (M = Mn, Co) showed much higher NO oxidation activity than Pt-based catalysts.[12] Thus it is significant to study the perovskite-based catalysts because they are much less expensive and more active towards NO oxidation than Pt-based catalysts.

Ba has been reported to be beneficial for the adsorption of NOx as nitrate.[19,20] Moreover, Liang *et al.* evaluated that Ba doped La–Ba–Ni mixed oxide catalysts for total oxidation of chlorinated hydrocarbons.[21] Compared with Ba free catalyst, Ba doping promoted the catalytic activity and $La_{0.5}Ba_{0.5}NiO_3$ exhibited the best performance. Bhavani *et al.* studied CO_2 reforming of methane by using Ba substituted $LaMnO_3$ perovskite and found that the optimal level of Ba substitution was 0.1 and 0.15 (Ba/Mn), which showed the highest CH_4 and CO_2 conversion, syngas selectivity and robust maintenance of these performances with little coke formation.[22] These investigations implied that the introduction of Ba into the perovskite structure might promote the catalytic performance. Co-based perovskite oxides were the most promising candidates as NO oxidation catalysts for its superior performance and the application of Ba doped $LaCoO_3$ in NO oxidation for emission control has not been studied. Hence in the present study, Ba-doped $LaCoO_3$ catalysts with different substitution levels for NO oxidation were investigated. It was found that Ba introduction improved the activity for NO oxidation dramatically and the maximum NO conversion was 93% at 265 °C for $La_{0.9}Ba_{0.1}CoO_3$, which exhibited much better performance than Pt-based catalysts (the

[a]*Ningbo Institute of Material Technology and Engineering, Chinese Academy of Sciences, Ningbo 315201, Zhejiang, People's Republic of China. E-mail: yinhf@nimte.ac.cn*

[b]*State Key Laboratory of Digital Manufacturing Equipment and Technology and School of Mechanical Science and Engineering, Huazhong University of Science and Technology, Wuhan 430074, Hubei, People's Republic of China. E-mail: bshan@hust.edu.cn*

[c]*State Key Laboratory of Material Processing and Die and Mould Technology and School of Materials Science and Engineering, Huazhong University of Science and Technology, Wuhan 430074, Hubei, People's Republic of China*

maximum conversion 62% at 320 °C). Our results indicated that Ba doped $LaCoO_3$ could be a candidate material as low cost and high performance for NO oxidation catalyst.

2. Experimental section

2.1 Catalyst synthesis

The Ba doped $LaCoO_3$ perovskite oxides were synthesized by a modified sol–gel method using citric acid (CA) and ethylenediamine tetraacetic acid (EDTA) as complexing agents, with an aqueous solution of each nitrate precursor (La, Ba, Co, Sr). The obtained gel was dried at 150 °C overnight and calcined at 700 °C for 5 hours in air prior to calcinations at 550 °C for 2 hours. 2% Pt/Al_2O_3 was also prepared *via* the wet-impregnation method as a reference.

In this paper, perovskite-type oxides with the formula $La_{1-x}Ba_xCoO_3$ ($x = 0, 0.1, 0.2, 0.3$) are hereafter named as LBC10 × x. For example, $La_{0.9}Ba_{0.1}CoO_3$ is abbreviated as LBC1.

2.2 Characterizations

X-ray diffraction (XRD) were performed to determine the phase structure of the synthesized catalysts, using a Bruker D8 Advance with a copper anode (Kα Cu = 1.54056 Å), operated an accelerating voltage of 40 kV and intensity of 40 mA at a step of 0.02° s^{-1} in the Bragg angle (2θ) range from 10° to 90°.

The inductively coupled plasma atomic emission spectrometry (ICP-AES) was conducted to measure the elementary chemical composition using a Perkin-Elmer Optima 2100.

The Brunauer–Emmett–Teller (BET) specific surface areas were determined *via* nitrogen absorption at 77 K using Micromeritics ASAP 2020M physisorption analyzer. Prior to the measurements, the catalysts were degassed at 200 °C for 5 hours.

The infrared spectra (FT-IR) of the oxides were collected on a Bruker Tensor 27 spectrometer in the range of 300–4000 cm^{-1} with a resolution of 4 cm^{-1} averaging 32 scans.

Transmission electron microscopy (TEM) and high-resolution transmission microscopy (HRTEM) images were analyzed with a JEM 2100 microscope operated at 200 kV.

The X-ray photoelectron spectroscopy (XPS) measurements were characterized on AXIS ULTRADLD multifunctional X-ray photoelectron spectroscope with an Al Kα radiation source at room temperature and the base pressure was 10^{-7} Pa (10^{-9} Torr).

H_2 temperature-programmed reduction (H_2-TPR) of the catalysts were carried out in a stream of 10% H_2–Ar mixture at a flow rate of 50 mL min^{-1} using FINESORB3010E instrument (Zhejiang Finetec Co.). For each H_2-TPR test, 30 mg of the catalysts placed in a U-type quartz tube reactor was pretreated at 300 °C for 1 hour under 21% O_2/N_2 stream and then cooled down to room temperature. During the H_2-TPR process, the sample was heated by increasing the temperature at a rate of 5 °C min^{-1}. The H_2 concentration in the effluent gas was determined by a thermal conductivity detector (TCD) with Ar gas as the reference gas.

For temperature-programmed desorption of NO (NO-TPD) experiment, 50 mg catalyst was pretreated in 10% O_2/N_2 at 500 °C for 1 hour and then cooled down to room temperature. And then the gas flow was switched to 500 ppm NO with N_2 as the balance after purging with N_2 for 30 minutes. Subsequently N_2 was introduced after the adsorption was finished. The catalyst was then heated up to 600 °C at a rate of 10 °C min^{-1} with pure 200 mL min^{-1} N_2. ECO physics chemiluminescent NOx analyzer (CLD822Mh), which can detect NO and NO_2 and the detect limit is 0.25 ppm, was used to detect the desorption species.

2.3 Activity test

Catalytic evaluation for NO oxidation was carried out in lean conditions by using the same reactor with temperature programmed experiment with 3 mm internal diameter of the reactor tube. 50 mg catalyst was used for each test, with the temperature measured by a K-type thermocouple in direct with the upper quartz wool near the powder. The gas mixture of 400 ppm NO, 10% O_2 and N_2 as the balance gas (150 mL min^{-1}) passed through the loaded catalyst. The space velocity was around 180 000 mL g^{-1} h^{-1}. The furnace was ramped at 2 °C min^{-1} from room temperature to 400 °C. The NO conversion was defined as the following formula:

$$\text{NO conversion}(\%) = \frac{NO_{in} - NO_{out}}{NO_{in}} \times 100$$

here, NO_{in} is the NO concentration in the inlet gas and NO_{out} is the NO concentration in the outlet gas.

3. Results and discussions

3.1 Structural characterizations

XRD patterns of the obtained LBC catalysts were shown in Fig. 1. $LaCoO_3$ behaved the typical hexagonal perovskite structure (JCPDS 25-1060). Note that the main peaks (110) around 2θ = 33° were split into two sub-peaks, indicating the rhombohedral distortion of the perovskite structure. For Ba-doped

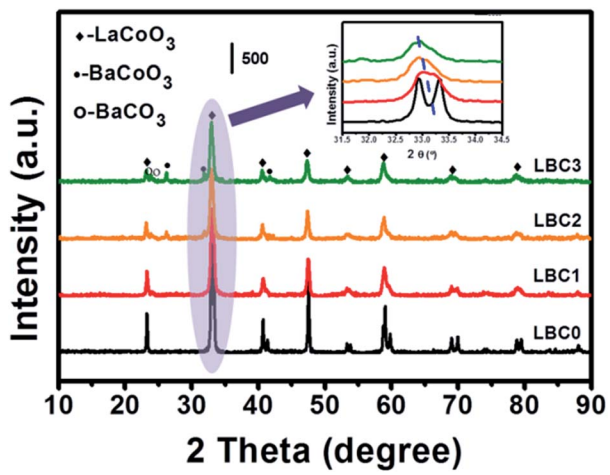

Fig. 1 XRD patterns of the LBC oxides.

catalysts, the two sub-peaks of main peak (110) were combined into one and shifted to lower 2θ angles. These demonstrated that Ba had been doped into the lattice structure and improved the symmetry of the perovskite structure. Similar phenomenon was also observed by Ca and Sr doped $LaCoO_3$ elsewhere.[14,23] The shift of main peak to lower 2θ angles suggested the lattice volume expansion as a result of larger ion radius of Ba^{2+} (1.35 Å) than that of La^{3+} (1.06 Å), which was in agreement with the results of Bhavani *et al.*[22] Meanwhile, the corresponding lattice parameters shown in Table 1, which were calculated according to the results of XRD, increased with increasing the doping content of Ba. Additionally, only the perovskite structure was observed in $LaCoO_3$ and a very weak diffraction peak of $BaCO_3$ was detected in LBC1. However, the diffraction peaks of $BaCoO_3$ (JCPDS 70-0363) and $BaCO_3$ (JCPDS 05-0378) were also observed for LBC2 and LBC3, implying some degree of phase segregation. The detailed phase composition on the basis of XRD patterns was shown in Table 2 as well. With increasing the addition of Ba, the content of $BaCO_3$ increased and the phase content of perovskite oxides including LBC and $BaCoO_3$ decreased. The ICP measurements displayed in Table 3 demonstrated that the intended compositions were nearly obtained.

BET specific area of the as-synthesized catalysts was also shown in Table 1. The BET surface area for LBC0 was 5.16 $m^2\ g^{-1}$, with those of Ba doped catalysts lied between 7.48 and 9.81 $m^2\ g^{-1}$. This demonstrated that the introduction of Ba into the perovskite structure improved the BET surface area of the catalysts.

Fig. 2 displayed the FT-IR results of the as-prepared $La_{1-x}Ba_xCoO_3$ perovskite oxides. For $LaCoO_3$, the spectrum bands at 598 cm^{-1} (very strong), 558 cm^{-1} (shoulder), 424 cm^{-1} (strong) and 343 cm^{-1} (strong) were observed. These bands were in consistent with the vibrational frequencies that corresponded to three normal modes reported by Merino *et al.*,[23] where the doublet bands at 598–558 cm^{-1} to the v1 mode, the band at 423 cm^{-1} to the v2 mode and the band at 329 cm^{-1} to the v4 mode. With the introduction of Ba into the A-site, the v1 mode with a shoulder became broader and weaker. Especially for LBC3 with the maximum Ba content the v1 mode became one band compared with Ba free sample $LaCoO_3$. Moreover, the intensity of v2 and v4 mode decreased when the Ba doping increased. The v4 mode band at 329 cm^{-1} was the O–Co–O angel deformation, which was usually inactive in IR for a cubic structure, but it was active in a distorted structure. The vibration of v1, v2 and v4 spectrum suggested that the substitution of La by Ba was in favor of improving the symmetry of the perovskite structure by transforming some amounts of Co^{3+} into Co^{4+}.[23] The interaction of Co^{4+} and O is stronger than that of Co^{3+} and O, thus the peak of the stretching vibration of Co^{4+}–O shifted to higher wavenumbers.[24] Thus the decrease intensity of Ba-doped samples showed that the substitution of Ba by La favored in improving the symmetry of the perovskite structure.[23] For LBC1, the bands at 857 cm^{-1} (weak), and 1432 cm^{-1} (strong) were detected. These bands were corresponded to the out-of-plane bending and the v3 mode of the carbonates,[25,26] respectively, which could come from the incomplete combustion of CA and EDTA. Except these, two new bands at 668 cm^{-1} and 693 cm^{-1} were observed on LBC2 and LBC3 as well. One band at 668 cm^{-1} was assigned to Co_3O_4 (the ABO_3 vibrations, where A denotes the Co^{2+} in a tetrahedral position).[24] This indicated that Co_3O_4 was generated when Ba doping content reached 20%. Another band at 693 cm^{-1} was attributed to in-plane bending mode of CO_3^{2-}.[25,26]

TEM and HRTEM images of LBC0 and LBC3 were displayed in Fig. 3. The particle sizes of the as-prepared catalysts lied between 40 nm and 60 nm. From HRTEM images of LBC0 (Fig. 3c), the displayed lattice spacing of 0.38 nm was corresponded to the (110) crystallite orientations of $LaCoO_3$. For LBC3 (Fig. 3d), other two crystal planes with the lattice spacing of 0.34 nm and 0.25 nm were also observed, which were corresponded to the (311) and (101) crystallite orientations of and $BaCoO_3$ and Co_3O_4, respectively. This confirmed that $BaCO_3$ and Co_3O_4 were existed on the LBC3 coincided with the results of FTIR. The failure to observe the Co_3O_4 phase from XRD could be ascribed to its small amount.

3.2 XPS

The surface compositions of the catalysts obtained from XPS analysis were listed in Table 4. The reactivity of perovskite was contributed to the active transition B ions reported by Voorhoeve *et al.*,[27,28] thus the surface content of B ions could be considered as an index correlating to the catalytic activity. As

Table 1 Lattice parameters and BET surface areas of the as-synthesized catalysts

Sample	a (Å)	c (Å)	BET surface area ($m^2\ g^{-1}$)
LBC0	5.4270	13.0802	5.16
LBC1	5.4402	13.1318	7.48
LBC2	5.4436	13.1421	8.79
LBC3	5.4450	13.1603	9.81

Table 2 The detailed phase composition on the basis of XRD results

Sample	LBC (wt%)	$BaCoO_3$ (wt%)	$BaCO_3$ (wt%)
LBC1	98.90 ± 0.1	0	1.10 ± 0.14
LBC2	88.25 ± 0.12	6.37 ± 0.14	5.38 ± 0.13
LBC3	81.57 ± 3.25	10.92 ± 0.39	7.50 ± 0.13

Table 3 ICP data (weight ratio) of the as-prepared catalysts; elemental composition with nominal values in parentheses

Sample	La [%]	Ba [%]	Co [%]
LBC0	56.06 (56.50)	0 (0)	23.53 (23.96)
LBC1	49.66 (50.47)	5.47 (5.54)	23.12 (23.78)
LBC2	44.14 (44.71)	10.52 (11.05)	22.64 (23.70)
LBC3	38.25 (38.98)	15.89 (16.51)	22.68 (23.62)

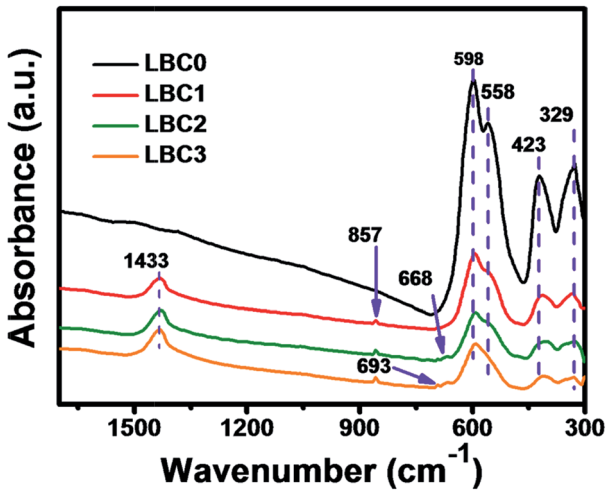

Fig. 2 FT-IR spectra of fresh LBC oxides.

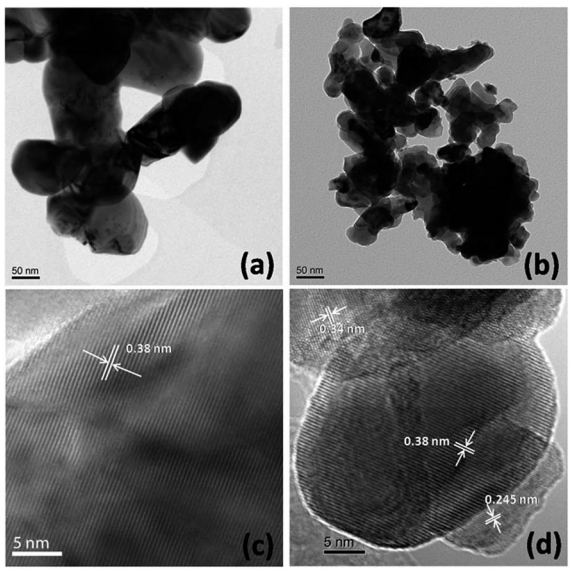

Fig. 3 TEM images and HRTEM images of LBC0 (a and c) and LBC3 (b and d).

Table 4 Surface components (atomic ratio) of the samples from XPS data (nominal values in parentheses)

Sample	La	Ba	Co (20)	O (60)
LBC0	16.16 (20)	—	11.61 (20)	71.67 (60)
LBC1	14.39 (18)	2.9 (2)	17.85 (20)	64.85 (60)
LBC2	12.7 (16)	3.24 (4)	20.72 (20)	63.34 (60)
LBC3	11.49 (14)	3.61 (6)	21.95 (20)	62.95 (60)

shown in Table 4, the surface Co content in LBC0 was 11.60 at% and the higher values were obtained for LBC1, LBC2 and LBC3, which were 17.85, 20.72, and 21.95 at%, respectively. This indicated that Ba substitution significantly increased the surface content of Co, indicating the surface segregation of Co. The content of Co on the surface was improved 53.8% with 10% Ba doping. This implied that Ba doping increased Co content on the surface, which could provide more active sites on the surface of the catalysts. With further increase of Ba content, the surface Co content was continued to increase. The extra amount of Co and Ba were in the form of $BaCO_3$, Co_3O_4 and $BaCoO_3$ existed on the surface and/or bulk of the catalysts.

3.3 H_2-TPR

The results of H_2-TPR were shown in Fig. 4, in which the reductions of Co_3O_4 (358 °C) and $BaCO_3$ (800 °C) were also given as the references. For LBC0, three reduction peaks were observed at 335 °C, 378 °C and 525 °C respectively. The former two peaks were attributed to the reduction of Co^{3+} to Co^{2+}, while the last peak at 525 °C was ascribed to the reduction of Co^{2+} to Co^0 in the perovskite structure of $LaCoO_3$.[29] For all Ba-doped samples, the reduction peaks shifted to lower temperatures. Three reduction peaks of LBC1 shifted to 283 °C, 324 °C and 496 °C, respectively, and much lower reduction temperatures were observed on LBC2 and LBC3. This might be attributed to the surface segregation of Co because of Ba substitution, which could facilitate the reduction with H_2. Especially, the reduction temperatures of Co^{3+} and Co^{2+} gradually approached to the reduction temperatures of Co_3O_4 (358 °C) with increasing the amount of Ba doping, underlying that the severe surface segregation of Co favored the formation of Co_3O_4 observed in HRTEM image (Fig. 3d) and FTIR (Fig. 2). Meanwhile, after Ba substitution, the starting reduction temperature began around 220 °C, which was much lower than that of $LaCoO_3$ (290 °C).

For each Ba-doped sample, additionally, anther reduction peak above 700 °C was observed. With increasing the amount of Ba, this peak was intensified and shifted to higher temperature approaching the reduction temperature of $BaCO_3$ (800 °C). This coincided in observation of $BaCO_3$ phase from XRD results of LBC2 and LBC3 (Fig. 1).

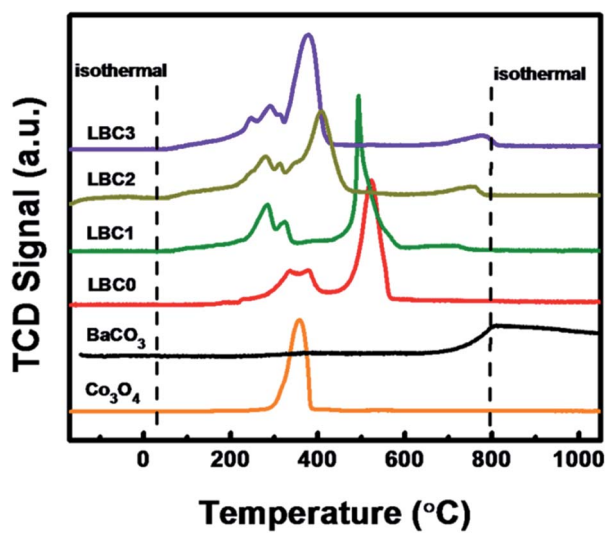

Fig. 4 H_2-TPR profile of the LBC oxide catalysts. The display values of Co_3O_4 were equal to the real values * 0.15.

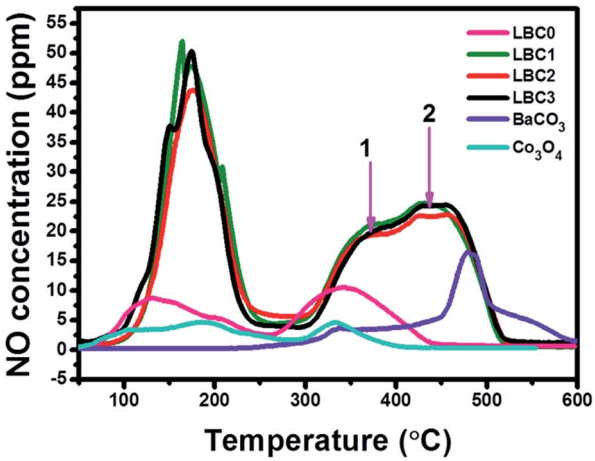

Fig. 5 NO-TPD patterns of the prepared LBC catalysts.

3.4 NO-TPD

The NO-TPD experiments were conducted to investigate the NO adsorption/desorption behavior over the $La_{1-x}Ba_xCoO_3$ catalysts. For LBC0, two desorption peaks, one below 250 °C and another at higher temperatures, were observed in Fig. 5. Wen *et al.*[30] demonstrated that three species were existed on $LaCoO_3$ including bridging nitrates, hyponitrite species and monodentate nitrates. The former two species disappeared up to 250 °C, which might be responsible to the desorption peak below 250 °C in Fig. 5, while the most stable monodentate nitrate to the desorption peak at higher temperatures.

For all Ba doped catalysts, the intensities of the two desorption peaks were both greatly became significant, indicating their higher capacities for NO adsorption. As listed in Table 5, the amount of NO desorption over Ba doped samples are above 110 μmol g^{-1}, much larger than that over LBC0 (35.3 μmol g^{-1}). Furthermore, the desorption temperatures of Ba-doped samples were also higher shown in Fig. 5, implying higher stabilities of adsorbed species. The Ba-doped samples for higher NO adsorption capacity might be ascribed to the stronger basicity of Ba.

As a reference, the desorption behaviour of NO on $BaCO_3$ and Co_3O_4 was also carried out. From Fig. 5, NO desorption was also observed for $BaCO_3$ (peak temperature at 480 °C) and Co_3O_4 (peak temperature at 185 °C and 334 °C) which indicated that both of them would absorb NO. This would explain that the desorption peak of Ba-doped catalysts became broader due to the formation of $BaCO_3$, Co_3O_4 and $BaCoO_3$ on the surface of the catalysts.

Table 5 Amounts of desorption NO of the as-synthesized catalysts

	Temperature range (°C)		
Sample	150–250 (μmol g^{-1})	250–600 (μmol g^{-1})	Total (μmol g^{-1})
LBC0	15.9	19.4	35.3
LBC1	56.8	62.1	118.9
LBC2	50.5	61.2	111.7
LBC3	55.1	59.7	114.8

3.5 Activity evaluation

The catalytic activity of the as-prepared catalysts towards NO oxidation was shown in Fig. 6, in which the thermodynamic equilibrium of NO to NO_2 was also given as a reference curve. The equilibrium conversion decreased with increasing the reaction temperature because the NO oxidation is an exothermic and reversible reaction. For $LaCoO_3$, NO conversion began to increase at 200 °C, and the maximum NO conversion of 77% was reached in the range of 310–320 °C. After that, the conversion dropped down because of thermodynamic limitations. For all Ba-doped samples, introduction of Ba into the perovskite structure promoted NO conversion dramatically, in which the light-off temperatures of NO conversion were shifted to *ca.* 150 °C and the maximums of NO conversion were greatly promoted at lower temperatures. Among these catalysts, LBC1 obtained the best performance with the maximum NO conversion of 93% at 265 °C. Further increase of Ba doping amount, the reactivity decreased slightly. However, it was still much higher than that of $LaCoO_3$. It is worth mentioning that all Ba-doped samples even behaved much higher activity than 2% Pt/Al_2O_3, and thus could be used as the potential substitutes for the noble metals-based catalysts. For pilot study, the activity of Co_3O_4 and $BaCoO_3$ were also given in Fig. 6, and the reactivity of different Co oxides towards NO oxidation followed the sequence: $LaCoO_3$ > Co_3O_4 > $BaCoO_3$. Note that with increasing Ba doping content, the content of the perovskite oxide LBC decreased (Table 2) and the content of Co on the surface of the catalysts increased (Table 4), but almost similar catalytic performance of LBC1, LBC2 and LBC3 was obtained. This might indicate that some composited interfaces such as LBC/Co_3O_4 were existed on the surface of the catalysts and the interaction between the perovskite oxides and Co_3O_4 had a greater contribution on the performance compared with pure LBC catalyst.

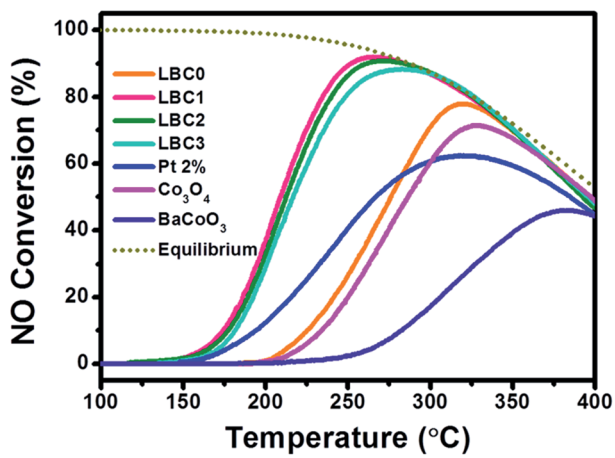

Fig. 6 NO removal percentage as a function of temperature and composition: 400 ppm NO, 10% O_2 and a balance of N_2.

4. Conclusions

Ba-doped $LaCoO_3$ were prepared readily by a modified sol–gel method. XRD, FTIR and H_2-TPR indicated that some segregation phases like $BaCO_3$, Co_3O_4 and $BaCoO_3$ were produced with increasing Ba doping content. Ba substitution for La in $LaCoO_3$ perovskite greatly improved the activity for NO oxidation. The best performance with the maximum NO conversion of 93% at 265 °C was observed on $La_{0.9}Ba_{0.1}CoO_3$. XPS demonstrated that Ba substitution led to the surface segregation of Co, which could promote the activity for NO oxidation. Moreover, all Ba-doped $LaCoO_3$ had better NO oxidation performance than that of the classical Pt/Al_2O_3 catalysts. This gave a hint that this kind of materials could be considered as the potential substituting candidate for noble metal-based catalysts and provided a viable direction for finding materials in good NO–NO_2 conversion with low cost.

Acknowledgements

This work is supported by the National Basic Research Program of China (2013CB934800 and 2011CB606401), National Natural Science Foundation of China (Grant 11004068, 21276262, 51101064 and 21307142), Fundamental Research Funds for the Central Universities, HUST (2012TS012 and 2012TS076), Ningbo Science and Technology Innovation Team Foundation (2014B81004) and China Postdoctoral Science Foundation (2012M521421). The authors acknowledge Thousand Young Talents Plan and New Century Excellent Talents in University (NCET) for providing grid resources that have contributed to the research results reported within this paper.

Notes and references

1 J. Chen, M. Shen, X. Wang, G. Qi, J. Wang and W. Li, *Appl. Catal., B*, 2013, **134–135**, 251.
2 J. Chen, M. Shen, X. Wang, J. Wang, Y. Su and Z. Zhao, *Catal. Commun.*, 2013, **37**, 105.
3 S. Roy and A. Baiker, *Chem. Rev.*, 2009, **109**, 4054.
4 P. Granger and V. I. Parvulescu, *Chem. Rev.*, 2011, **111**, 3155.
5 X.-G. Li, Y.-H. Dong, H. Xian, W. Y. Hernandez, M. Meng, H.-H. Zou, A.-J. Ma, T.-Y. Zhang, Z. Jiang, N. Tusbaki and P. Vernoux, *Energy Environ. Sci.*, 2011, **4**, 3351.
6 C. Constantinou, W. Li, G. Qi and W. S. Epling, *Appl. Catal., B*, 2013, **134–135**, 66.
7 W. Hauptmann, M. Votsmeier, J. Gieshoff, A. Drochner and H. Vogel, *Appl. Catal., B*, 2009, **93**, 22.
8 L. Olsson and E. Fridell, *J. Catal.*, 2002, **210**, 340.
9 P. Forzatti, L. Lietti, I. Nova and E. Tronconi, *Catal. Today*, 2010, **151**, 202.
10 G. R. Moradi and M. Rahmanzadeh, *Catal. Commun.*, 2012, **26**, 169.
11 J. A. Villoria, M. C. Alvarez-Galvan, S. M. Al-Zahrani, P. Palmisano, S. Specchia, V. Specchia, J. L. G. Fierro and R. M. Navarro, *Appl. Catal., B*, 2011, **105**, 276.
12 C. H. Kim, G. Qi, K. Dahlberg and W. Li, *Science*, 2010, **327**, 1624.
13 Y. Liu, H. Dai, Y. Du, J. Deng, L. Zhang, Z. Zhao and C. T. Au, *J. Catal*, 2012, **287**, 149.
14 S.-T. Shen and H.-S. Weng, *Ind. Eng. Chem. Res.*, 1998, **37**, 2654.
15 C. Batiot-Dupeyrat, G. Valderrama, A. Meneses, F. Martinez, J. Barrault and J. M. Tatibouët, *Appl. Catal., A*, 2003, **248**, 143.
16 R. J. H. Voorhoeve, J. P. Remeika, P. E. Freeland and B. T. Matthias, *Science*, 1972, **177**, 353.
17 Y. Wang, J. Ren, Y. Wang, F. Zhang, X. Liu, Y. Guo and G. Lu, *J. Phys. Chem. C*, 2008, **112**, 15293.
18 C. Zhou, X. Liu, C. Wu, Y. Wen, Y. Xue, R. Chen, Z. Zhang, B. Shan, H. Yin and W. G. Wang, *Phys. Chem. Chem. Phys.*, 2014, **16**, 5106.
19 H. Xian, X. Zhang, X. Li, L. Li, H. Zou, M. Meng, Q. Li, Y. Tan and N. Tsubaki, *J. Phys. Chem. C*, 2010, **114**, 11844.
20 L. Olsson, B. Westerberg, H. Persson, E. Fridell, M. Skoglundh and B. Andersson, *J. Phys. Chem. B*, 1999, **103**, 10433.
21 C. Liang, C. Ku, Y. Chen and J. Liang, *Catal. Commun.*, 2012, **17**, 43.
22 A. G. Bhavani, W. Y. Kim and J. S. Lee, *ACS Catal.*, 2013, **3**, 1537.
23 N. A. Merino, B. P. Barbero, P. Grange and L. E. Cadús, *J. Catal.*, 2005, **231**, 232.
24 H. Wang, Z. Zhao, P. Liang, C. Xu, A. Duan, G. Jiang, J. Xu and J. Liu, *Catal. Lett.*, 2008, **124**, 91.
25 M. Motta, C. V. Deimling, M. J. Saeki and P. N. Lisoba-Filho, *J. Sol-Gel Sci. Technol.*, 2008, **46**, 201.
26 L. Chen, Y. Shen, A. Xie, J. Zhu, Z. Wu and L. Yang, *Crsyt. Res. Technol.*, 2007, **42**, 886.
27 R. J. H. Voorhoeve, J. P. Remeika and L. E. Trimble, *Ann. N. Y. Acad. Sci.*, 1976, **272**, 3.
28 R. J. H. Voorhoeve, D. W. Johnson, J. P. Remeika and P. K. Gallagher, *Science*, 1977, **195**, 827.
29 N. Mota, M. C. Álvarez-Galván, J. A. Villoria, F. Rosa, J. L. G. Fierro and R. M. Navarro, *Top. Catal.*, 2009, **52**, 1995.
30 Y. Wen, C. Zhang, H. He, Y. Yu and Y. Teraoka, *Catal. Today*, 2007, **126**, 400.